Collective Multivortex States in Periodic Arrays of Traps

Charles Reichhardt
Department of Physics, University of California, Davis, California 95616

Niels Grønbech-Jensen
Department of Applied Science, University of California, Davis, California 95616
and NERSC, Lawrence Berkeley National Laboratory, Berkeley, California 94720
(Received 12 April 2000)

We examine the vortex states in a 2D superconductor interacting with a square array of pinning sites. As a function of increasing pinning size or strength we find a series of novel phases including multivortex and composite superlattice states such as aligned dimer and trimer configurations at individual pinning sites. Interactions of the vortices give rise to an orientational ordering of the internal vortex structures in each pinning site. We also show that these vortex states can give rise to a multistage melting behavior.

PACS numbers: 74.60.Ge, 74.60.Jg

Vortex lattice states in periodic pinning arrays have recently been attracting considerable attention as they represent ideal examples of an elastic lattice interacting with a periodic substrate. Experiments with periodic pinning arrays using microholes [1,2], blind holes [3,4], and magnetic dot arrays [5], as well as simulations [6], have found numerous commensurability effects in which the pinning is enhanced at applied fields where the number of vortices equals an integer or rational fraction of the number of pinning sites. Direct imaging using Lorentz microscopy, of these commensurate vortex lattice structures in periodic pinning arrays, in which only one vortex is trapped at a single pinning site, has been conducted by Harada *et al.* [2] where a remarkable variety of different kinds of ordered vortex crystals was found. These experiments also show that, for vortex densities greater than the first matching field, vortices can be positioned in the interstitial regions between the vortices trapped at the pinning sites.

Another possibility at the matching fields is that *multiple* vortices can occupy individual pinning sites. Bitter decoration experiments by Bezryadin *et al.* [3,4] have shown multivortex states in which up to nine vortices can be trapped at a single site. The individual vortices in the pinning sites are observed to form various types of structures and position themselves as far apart as possible to reduce their repulsive interaction energy. This work also demonstrates that for smaller pinning sites there can be a coexistence between multivortex states at the pinning sites with interstitial vortices between the pinning sites. As the pinning size is increased the number of vortices trapped at a single site also increases. Several other experiments have interpreted magnetization and creep measurements in terms of multivortex and composite vortex states.

Vortex states in single large pinning sites and mesoscopic disks have also been studied [7–11]. Khalfin and Shapiro [7] have predicted the vortex patterns for an increasing number of fluxons in large pinning sites which are similar to those observed in experiments [3,4]. Multivortex states and configurations in thin superconducting disks can have preferred structures for a specific number of vortices that are captured [10,11]. Similar systems of repulsive particles in a confining potential include electron crystals in Coulomb islands [12] and colloids in parabolic traps [13].

Despite the work done on vortex configurations in a single defect or disk the case of multivortex configurations in coupled arrays of defects has not been addressed. In this work we show through numerical simulations of logarithmically interacting vortices in 2D superconductors that as a function of pinning size and strength a series of novel collective multivortex and composite vortex lattice states can be realized. The long-range interactions of the vortices causes the vortex structures internal to the pinning sites to give rise to an orientational ordering with respect to the vortex structures in the other pinning sites. Such states include orientationally ordered dimer, trimer, and composite states. Transitions between different vortex states can be observed as jumps in the critical depinning force as a function of pinning size. We also show that in these systems multistage melting processes can occur where the orientational degrees of freedom of the internal vortex lattice structure in the pinning sites melt at a much lower temperature than the whole vortex lattice does. Particular systems in which these states can be realized include thin-film superconductors with arrays of blind holes, disks, or weak magnetic dots. Other possible physical realizations include charged colloidal particles or Wigner crystals in 2D trap arrays.

We consider a 2D system with periodic boundary conditions. We numerically integrate the overdamped equation of motion for a vortex i,

$$\eta \frac{d\mathbf{r}_i}{dt} = \mathbf{f}_i = \mathbf{f}_i^{vv} + \mathbf{f}_i^{vp}. \tag{1}$$

The vortex-vortex interaction potential is chosen to be logarithmic $U_v = -\ln(r)$. The force on vortex i

 0031-9007/00/85(11)/2372(4)$15.00

from the other vortices is $\mathbf{f}_i^{vv} = -\sum_{j\neq i}^{N_v} \nabla_i U_v(r_{ij})$, where $r_{ij} = |\mathbf{r}_i - \mathbf{r}_j|$ is the distance between vortices i, j, and η is the Bardeen-Stephen friction. We evaluate the periodic long-range logarithmic interaction with the resummations given in Ref. [14]. The pinning is modeled as a square array of attractive parabolic wells with $f_i^{vp} = -\sum_{k=1}^{N_p} \times (f_p/r_p)\Theta(r_p - |\mathbf{r}_i - \mathbf{r}_k^{(p)}|)\hat{\mathbf{r}}_{ik}^{(p)}$. Here Θ is the step function, $\mathbf{r}_k^{(p)}$ is the location of pinning site k, f_p is the maximum pinning force, and r_p is the radius of the pinning site. To obtain vortex configurations we start from a high temperature where the vortices are in a molten state and gradually cool until $T = 0$. We have verified that our cooling rate is sufficiently slow so that the final state no longer depends on the cooling rate. In this Letter we focus on the case of $B/B_\phi = 2$, 3, and 4, where B_ϕ is the field at which there is one vortex per pinning site. This is adequate to capture the general features of the vortex states for higher matching fields. Results for higher B/B_ϕ and incommensurate filling fractions will be presented elsewhere. The results for this work are for 8×8 pinning arrays. We have also conducted simulations with larger systems and for different pinning lattice constants and have found the same features as seen for the 8×8 systems. When the pinning sites are sufficiently large, multiple vortices can be captured per pinning site. We note that it is possible that vortices in the pinning sites can for certain parameters form individual giant vortex states [10] which we do not consider here.

In Fig. 1 we show the four vortex states that are possible for $B/B_\phi = 3.0$ for varying pinning strength and size. In Fig. 1(a) for the weak $f_p = 0.25$ and small pinning $r_p = 0.15$ the vortex-vortex interactions dominate and the vortex lattice forms a nearly *triangular* lattice. The vortex lattice still takes advantage of the pinning; however, only *half* the pinning sites can be occupied in order for the vortex lattice to have triangular ordering. We label this phase the commensurate elastic lattice. In Fig. 1(b), for stronger pinning, the pinning sites each capture one vortex and the vortex lattice is no longer triangular. The overall vortex lattice is still ordered with pairs of interstitial vortices alternating in positions. The state in Fig. 1(b) is identical to the state observed experimentally by Harada *et al.* [2] for the third matching field. For increased pinning radius $r_p = 0.5$, and $f_p = 1.25$, in Fig. 1(c) each pinning site can capture two vortices giving rise to a composite lattice of multivortices at the pinning sites and interstitial vortices. The vortices in the pinning sites repel one another and move to the edges of the pinning site. The interactions between the vortices in the pinning sites with the vortices in the other pinning sites give rise to an orientational ordering between the dimers with a rotation of 45° from one another. The interstitial vortices also form a periodic distorted square sublattice with unit cell for the overall vortex lattice, outlined in Fig. 1(c), consisting of

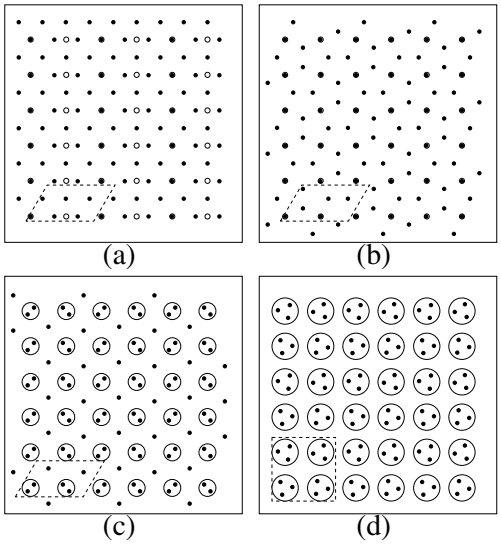

FIG. 1. Vortex states and unit cells for $B/B_\phi = 3.0$ for a 6×6 subsection. (a) $f_p = 0.25, r_p = 0.15$ shows a nearly triangular vortex lattice. (b) $f_p = 1.25, r_p = 0.15$. (c) $f_p = 1.25, r_p = 0.5$. Every pinning site captures two vortices forming a dimer state with the dimers being orientationally ordered with respect to one another, as well as with the interstitial vortices. (d) $f_p = 1.25, r_p = 0.8$. Every pinning site captures three vortices forming a trimer state with the trimers orientationally ordered as seen in the unit cell.

two dimers and two interstitial vortices. In Fig. 1(d) for larger $f_p = 1.25$ and $r_p = 0.8$, each pinning site captures three vortices with the vortices forming triangles inside the pinning wells, producing a trimer state. The vortices in the pinning site again show nontrivial ordering with respect to each other. The vortex structures in alternating rows of pinning sites are rotated about 40° from one another. Additionally the vortex structures in every other pinning site in the same row show a smaller rotation by about 5°. The unit cell as outlined in Fig. 1(d) consists of four pinning sites and 12 vortices.

In Fig. 2 we show the evolution of the vortex states for $B/B_\phi = 4.0$ for increasing pinning size and strength. We again observe four vortex states. For weak and small pinning sites [Fig. 2(a)], $f_p = 0.25, r_p = 0.15$, only one vortex is captured per pinning site with the overall vortex lattice having a slightly distorted triangular ordering. We do not find a state where only a fraction of the vortices are filled, as in region I for $B/B_\phi = 3.0$, which can be understood by considering that in Fig. 2(a) the vortex lattice is already triangular. The state in Fig. 2(a) was also observed in experiments [2]. In Fig. 2(b) where two vortices can be captured we do not find a completely ordered overall lattice. Here the lattice breaks up into domains with two separate orientations. This can be a finite size effect where the 8×8 system is incommensurate with the unit cell of order. In Fig. 2(c) three vortices are captured per pinning site where the trimers are oriented with respect to one another and the interstitial vortices form a square sublattice.

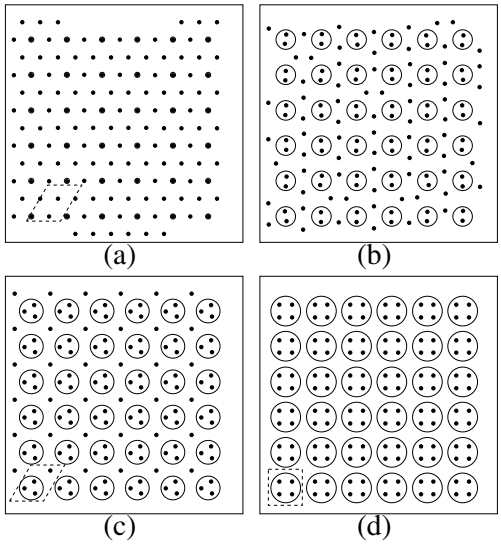

FIG. 2. Vortex states and unit cells for $B/B_\phi = 4.0$ for a 6×6 subsection. (a) $f_p = 0.25, r_p = 0.15$. Every pinning site captures one vortex with the overall lattice having a triangular ordering. (b) $f_p = 1.25, r_p = 0.6$. Every pinning site captures two vortices. The overall vortex lattice is not ordered but broken into domains. (c) $f_p = 1.25, r_p = 0.75$. Every pinning site captures three vortices forming a collective, trimer state with the interstitial vortices forming a square sublattice. (d) $f_p = 1.25, r_p = 0.85$. Every pinning site captures four vortices with the vortices in the pinning sites forming an aligned square lattice.

In Fig. 2(d) where each pinning site captures four vortices, the vortices in the pinning sites form a square lattice with the same orientation as the pinning lattice.

We have also conducted simulations for $B/B_\phi > 4.0$ and observe the same general features of the vortex states as outlined above, in particular, the orientational ordered multivortex lattice states and ordered interstitial sublattices. The number of different kinds of states increases with the field.

In Fig. 3(a) we show the evolution of the phases for the $B/B_\phi = 3.0$ case for varied r_p and f_p with regions I through IV corresponding to the phases in Figs. 1(a)–1(d). As r_p and f_p are increased region II slowly decreases, region III maintains a roughly constant width, and region IV grows. Region I disappears for $f_p > 1.0$. In Fig. 4(b) we plot the evolution of the phases for $B/B_\phi = 4.0$ with regions I′ through IV′ corresponding to the phases in Figs. 2(a)–2(d). Here region I′ is considerably larger than the other phases. For increasing f_p region IV′ grows while regions II and III keep roughly the same width.

The onset of the different vortex states as a function of r_p at constant f_p can also be observed as discrete jumps in the critical depinning force. The depinning is determined by adding an increasing driving force term to Eq. (1) in the symmetry direction of the pinning lattice and monitoring when the vortex velocities become nonzero.

In Fig. 4 we show that the collective multivortex states can give rise to a novel multistage melting behavior. We focus here on the simplest collective multivortex state at

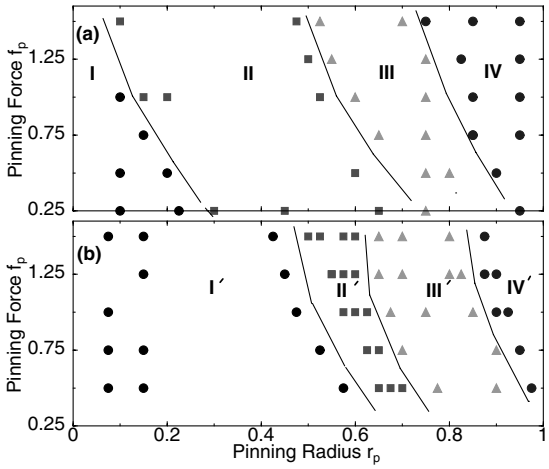

FIG. 3. The phase diagram for (a) $B/B_\phi = 3.0$ and (b) $B/B_\phi = 4.0$ for varied r_p and f_p. The regions I through IV correspond to phases (a)–(d) in Fig. 1 and regions I′ through IV′ correspond to phases (a)–(d) in Fig. 2.

$B/B_\phi = 2.0$, when there are two vortex states. In the first state, every pinning site captures one vortex while interstitial vortices form a square sublattice as previously observed in simulations [6] and experiments [2]. The second state, shown in Fig. 4(a), is an aligned dimer state with all the vortex dimers being aligned at 45°. We apply a temperature by adding Gaussian noise to Eq. (1). The dimers stay aligned until $T = 0.004$ at which point they begin to freely rotate inside the wells as shown in the vortex trajectories in Fig. 4(c). This destroys the orientational order, as seen in Fig. 4(b), and results in a liquid dimer state. As T is increased the vortices remain confined in the pins until $T = 0.01$ when the overall lattice melts with vortices diffusing randomly in the sample as shown in Fig. 4(d). To measure the melting transitions quantitatively in Fig. 4(e) we plot the angular correlation of the dimers $C_\theta = \langle \sum_{nm} \exp[2i(\theta_n - \theta_m)] \rangle / N$. We also plot a measure of the vortex displacements from their initial position at $T = 0$ and compared to the displacements at a higher T: $d(T) = [r(\tau) - r(0)]^2$. Here τ is the time interval between temperature increments. For low T, C_θ is near unity and $d(T) \approx 0$ as the dimers remain aligned. At $T = 0.004$, the dimers begin to freely rotate, as seen in the drop in C_θ to ≈ 0.3 (notice that C_θ would be close to zero for a large system simulated over a long time), as well as the finite jump in $d(T)$. Since the dimers are still confined to the pinning wells $d(T)$ stays at a constant value in the molten dimer state. For $T > 0.09$ $d(T)$ rises rapidly as the vortices begin to jump out of the wells and diffuse randomly in the liquid state. The melting temperature of the dimer states is reduced as the pinning lattice constant is increased or the pinning radius is reduced. For higher matching fields a similar multistage melting behavior is observed where the loss of orientational ordering of the vortices in the pinning sites occurs before the loss of order in the overall lattice. More work is needed to

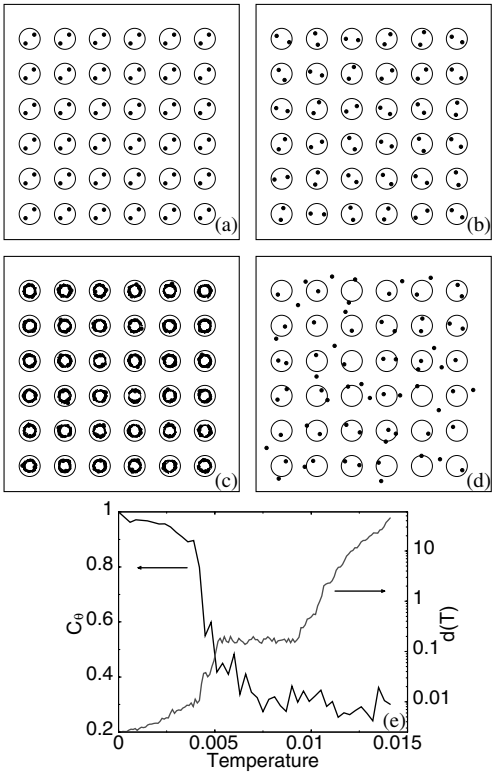

FIG. 4. The vortex positions for $B/B_\phi = 2.0$ for (a) $T = 0.0$, the collective dimer state. (b) $T = 0.006$, the liquid dimer state, where the orientational ordering between the dimers is lost. The vortex trajectories for $T = 0.006$ are shown in (c) where the dimers can be seen to rotate inside the pinning sites. (d) The vortex liquid state, $T = 0.0125$, as vortices diffuse throughout the sample. In (e) the orientational correlation function C_θ for the dimer and the vortex displacements $d(T)$ for increasing T. The aligned dimer state is molten $T > 0.004$ and the overall lattice melts for $T > 0.009$ as seen in the large increase in the $d(T)$.

determine the nature of the melting of the dimer or trimer states, such as whether it is continuous and similar to the melting in XY-type models. It may also be possible that additional melting stages occur when the vortices are still inside the pinning site similar to the melting behaviors of vortices [8] or colloids [13] inside individual traps.

We point out that in addition to simulations with logarithmically interacting vortices we have also conducted 2D simulations with a finite range Bessel function interaction and find (provided the interaction range is sufficiently large) similar features in the vortex structures and multistage melting indicating that many of the phases we observed here are general features of systems of 2D repulsive particles in periodic arrays.

In conclusion we have studied the vortex states in thin-film superconductors interacting with periodic pinning arrays in which multiple vortices can be trapped at individual sites. We find that a rich variety of novel vortex states is possible as a function of pinning strength and pinning size. These states include collective dimer, trimer, and composite states in which the vortex structures in the pinning sites exhibit an orientational ordering with each other. Transitions between the different states can be observed as a series of discrete jumps in the critical depinning force for varied pin radius. We also show that these systems exhibit a multistage melting where the structures internal to the vortex lattice melt before the overall vortex lattice melts. Besides vortices in superconductors these states may be observable for charged colliods in multitrap arrays.

We thank C. J. Olson for a critical reading of this manuscript and G. T. Zimanyi, R. T. Scalettar, and F. Nori for useful discussions. This work was supported by the Director, Office of Advanced Scientific Computing Research, Division of Mathematical, Information and Computational Sciences of the U.S. Department of Energy under Contract No. DE-AC03-76SF00098, as well as CLC and CULAR (Los Alamos National Laboratory).

[1] M. Baert *et al.,* Phys. Rev. Lett. **74**, 3269 (1995); J. Y. Lin *et al.,* Phys. Rev. B **54**, R12 717 (1996); A. Castellanos *et al.,* Appl. Phys. Lett. **71**, 962 (1997); V. V. Moshchalkov *et al.,* Phys. Rev. B **57**, 3615 (1998); V. V. Metlushko *et al.,* Europhys. Lett. **41**, 333 (1998); V. V. Metlushko *et al.,* Phys. Rev. B **59**, 603 (1999); L. Van Look *et al.,* Phys. Rev. B **60**, R6998 (1999); S. Field *et al.,* cond-mat/0003415.

[2] K. Harada *et al.,* Science **271**, 1393 (1996).

[3] A. Bezryadin and B. Pannetier, J. Low Temp. Phys. **102**, 73 (1996).

[4] A. Bezryadin, Yu. N. Ovchinnikov, and B. Pannetier, Phys. Rev. B **53**, 8553 (1996).

[5] J. I. Martín *et al.,* Phys. Rev. Lett. **79**, 1929 (1997); D. J. Morgan and J. B. Ketterson, Phys. Rev. Lett. **80**, 3614 (1998); A. Terentiev *et al.,* Physica (Amsterdam) **324C**, 1 (1999); M. K. Van Bael *et al.,* Phys. Rev. B **59**, 14 674 (1999); J. I. Martín *et al.,* Phys. Rev. Lett. **83**, 1022 (1999); Y. Fasano *et al.,* Phys. Rev. B **60**, R15 047 (1999); A. Hoffmann, P. Prieto, and I. K. Schuller, Phys. Rev. B **61**, 6958 (2000); A. Terentiev *et al.,* Phys. Rev. B **61**, R9249 (2000).

[6] C. Reichhardt, C. J. Olson, and F. Nori, Phys. Rev. B **57**, 7937 (1998); C. Reichhardt *et al.* (to be published).

[7] I. B. Khalfin and B. Ya. Shapiro, Physica (Amsterdam) **202C**, 393 (1992); A. I. Buzdin, Phys. Lett. A **196**, 267 (1994).

[8] Yu. E. Lozovik and E. A. Rakoch, Phys. Rev. B **57**, 1214 (1998).

[9] A. K. Geim *et al.,* Nature (London) **390**, 259 (1997).

[10] V. A. Schweigert, F. M. Peeters, and P. Singha Deo, Phys. Rev. Lett. **81**, 2783 (1998).

[11] P. S. Deo *et al.,* Phys. Rev. Lett. **79**, 4653 (1997); J. J. Palacios, Phys. Rev. B **58**, R5948 (1998).

[12] A. A. Koulakov and B. I. Shklovskii, Phys. Rev. B **57**, 2352 (1998).

[13] R. Bubeck *et al.,* Phys. Rev. Lett. **82**, 3364 (1999).

[14] N. Grønbech-Jensen, Int. J. Mod. Phys. C **7**, 873 (1996); Comput. Phys. Commun. **119**, 115 (1999).